FULL PAPER

Semi-Egg-Like Heterogeneous Compartmentalization of Cells Controlled by Contact Angle Hysteresis

*Kang Sun, Mingjie Liu, Hongliang Liu, Pengchao Zhang, Junbing Fan, Jingxin Meng, and Shutao Wang**

Precise control of liquid inside compartments is critically important in bioreactors, combinatorial analysis, and tissue engineering. A contact angle hysteresis (CAH)-based strategy is demonstrated to construct a semi-egg-like hydrogel architecture, leading to spatial heterogeneous compartmentalization of cells. The semi-egg-like architecture is fabricated by successively capturing and gelling prehydrogel liquids using a substrate with controlled-CAH pattern and ultralow-CAH background. The controlled-CAH pattern could capture liquid with tunable size, while ultralow-CAH background prevents liquid sticking. It is envisioned that this CAH-based strategy would be promising in designing functional surface for engineering complicated architectures of either biomedical or nonbiomedical systems.

1. Introduction

Compartmentalization of liquid on solid surface is an important issue closely related to high-throughput screening,[1] microlens array,[2] and bioreactors.[3] Current methods for liquid compartmentalization mainly include geometrical confinement[1,4] and patterning surface with wettability contrast.[5–8] For closed systems, the geometrical confinement approach is mostly applied in which liquid is confined in geometrically designed compartments. For open systems, patterning surface with wettability contrast is widely adopted through a controlled wetting/dewetting process. These methods achieve liquid compartmentalization with liquid filling the predesigned compartments. However, it is still a challenge to precisely control liquid inside compartments, e.g., tuning size of liquids, which is useful in varying crystallization conditions and engineering stem cell spheroids.[9,10] Herein, we attempt to control size of liquids in compartments by utilizing contact angle hysteresis (CAH), which affects dynamic wetting/dewetting of liquid on surface.[11–15] In daily life and industrial applications, large CAH is generally an unfavorable factor that causes pinning of droplets, resulting in failure of self-cleaning surfaces,[16,17] lowering the production yield in immersion lithography,[18] and contributing to coffee strain effects in inkjet printing.[19] However, CAH has also been shown to modulate actuation of droplet[20] and affect self-assembly of nanoparticles.[21] Thus, utilization of CAH could pave more paths to engineering the compartmentalization of various fluids, including biocompatible liquid for biomedical applications.[22]

Native tissues are hierarchical assemblies of heterogeneous types of cells and extracellular matrix across multiple length scales. In tissue engineering, it is essential to control the size of cell aggregates, or cell-encapsulated matrix (e.g., hydrogel) for mimicking conditions in vivo. Compartmentalization of different cells into specific architectures would benefit studying differentiation of stem cells, fabricating artificial niche for perturbing stem cell fates, and investigating biological performance for cells arranged in tissue scale.[23–25] Herein, we report a CAH-based strategy to construct a cell-encapsulated semi-egg-like hydrogel architecture by controlling size of different prehydrogel solutions in compartments followed by rapid gelation (**Scheme 1**). We fabricated a substrate with controlled-CAH pattern and ultralow-CAH background, and compartmentalized liquid with controlled sizes. Following a simple two-step dip-coating, a semi-egg-like architecture with encapsulated cells was fabricated. The cell encapsulated semi-egg-like structure was used as a model for evaluating cell viability when exposed to oxidative stress. We believe that this CAH-based strategy could be useful in various applications that involve compartmentalizing liquid and constructing complicated hydrogel structures.

2. Results and Discussion

2.1. Fabrication Silicon Substrates with Various CAH

We first fabricated substrates with controlled CAH by etching silicon in various $AgNO_3$ and HF solutions.[26] As shown in **Figure 1**, roughness of substrates varies for different etching conditions. We obtained 0.20, 1.30, 2.03, 3.87, 6.23, and 9.40 nm (root-mean-square roughness, R_{rms}) for solutions with concentrations 0, 0.2, 0.4, 0.6, 0.8, and onefold of original solution (Figure S1, Supporting Information). The high concentration of

Dr. K. Sun, Dr. H. Liu, Dr. J. Fan,
Dr. J. Meng, Prof. S. Wang
Laboratory of Bio-inspired Smart Interface Science
Technical Institute of Physics and Chemistry
Chinese Academy of Sciences
Beijing 100190, P. R. China
E-mail: stwang@mail.ipc.ac.cn
Dr. K. Sun, Dr. M. Liu, Dr. P. Zhang
Beijing National Laboratory for Molecular Sciences (BNLMS)
Key Laboratory of Organic Solids
Institute of Chemistry
Chinese Academy of Sciences
Beijing 100190, P. R. China

DOI: 10.1002/adfm.201501527

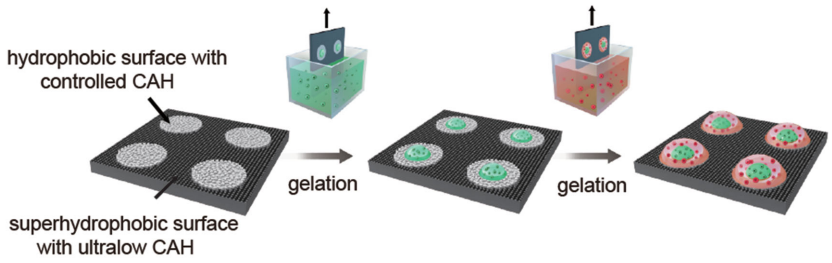

Scheme 1. Contact angle hysteresis (CAH)-based generation of cell encapsulated hydrogel with semi-egg-like architecture. A substrate with controlled CAH on pattern area and ultralow CAH in background was fabricated. Primary dip-coating and gelation generated patterned droplets with controlled size. Secondary dip-coating and gelation generated the semi-egg-like architecture.

etching solution provides more deposited Ag nanoparticles as etching sites compared to the low ones, resulting in a rougher surface.[27] We measured the static contact angles (θ), advancing contact angles (θ_A), and receding contact angles (θ_R) of different substrates after modification with octadecyltrichlorosilane (OTS) (Figure 1b). θ and θ_A of substrates increased with the increase of roughness, while θ_R decreased with increase of roughness. As a result, the calculated CAH ($\theta_A - \theta_R$) increased in response to surface roughness (Figure 1c). We obtained the largest CAH ≈58° for substrate with R_{rms} 9.40 nm, and the smallest ≈10° for substrate without etching. Apart from $\theta_A - \theta_R$, CAH is also evaluated by the difference between cosine of receding and advancing contact angles ($\cos\theta_R - \cos\theta_A$). For liquid on surface, in three-phase contact line, the force per unit length required to move the contact line is defined by

$$F = \gamma(\cos\theta_R - \cos\theta_A) \quad (1)$$

in which γ is the liquid surface tension.[11] For a given liquid, hysteresis force F is proportional to $\cos\theta_R - \cos\theta_A$. The calculated $\cos\theta_R - \cos\theta_A$ in our experiments showed a positive relationship with roughness (Figure 1c, inset). The tunable CAH implies the ability to control hysteresis force that hinders liquid motion on surface.

2.2. Compartmentalization of Liquids with Controlled Size

To achieve liquid compartmentalization, we fabricated silicon substrate with controlled-CAH patterns and ultralow CAH background (Figure S2, Supporting Information). The ultralow CAH background was achieved by a further etching in the background. After modification with OTS, static contact angle of the background was >150°, and CAH was <5° (Figure S3, Supporting Information), showing that the background was superhydrophobic with an ultralow CAH. Using this controlled-CAH/ultralow-CAH substrate, we obtained size-controlled water and viscous solution droplets by dip-coating (**Figure 2**). For convenience, projected areas of droplets on pattern were measured to characterize the droplet size. For water, droplet size increased with the increase of CAH (shown in the form of $\cos\theta_R - \cos\theta_A$ to reveal hysteresis force). For substrates with CAH smaller than 0.53 ± 0.04, droplets disappeared quickly due to evaporation (Figure S4, Supporting Information). For CAH larger than 0.53 ± 0.04, larger droplets remained unchanged on the patterns during imaging. For viscous solution, we employed sodium alginate solution (ALG-Na). ALG-Na powder is a common industrial thickener.[28] Its hydrogel is widely used as

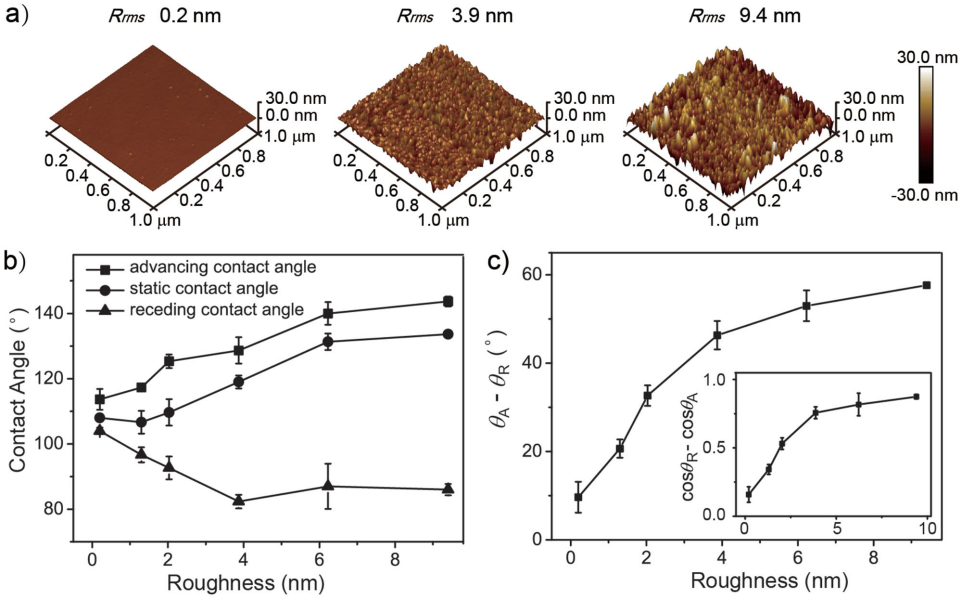

Figure 1. Tuning CAH by surface roughness. a) Surface roughness increased with the increase of concentrations of etching solutions. b) Static contact angle θ, advancing contact angle θ_A, and receding contact angle θ_R in response to different roughness. c) Calculated $\theta_A - \theta_R$ increased with the increase of roughness. Inset: calculated ($\cos\theta_R - \cos\theta_A$) increased with the increase of roughness.

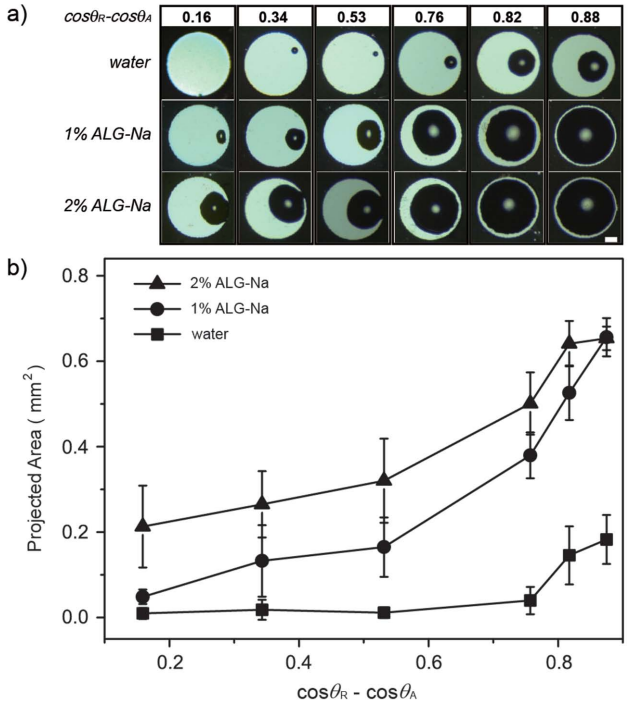

Figure 2. Control of droplet size using controlled-CAH/ultralow-CAH substrate. To imply the hysteresis force during dip-coating, $\cos\theta_R - \cos\theta_A$ is used instead of $\theta_A - \theta_R$ here. a) Optical images of liquid droplets (deionized water, 1% ALG-Na, and 2% ALG-Na) formed on patterns with various CAH. b) Droplet size measured (represented in the form of projected area) as a function of CAH. For the same liquid, the size generally increased with the increase of CAH. For the same substrate, size increased with liquid concentration. Scale bar: 200 μm.

cell culture matrices.[29] We prepared ALG-Na solutions (in phosphate buffered saline) with various concentrations. Viscosity of solutions was shown in Table S1 (Supporting Information). Figure 2 shows for both 1% and 2% solution, droplet size increased with the increase of CAH. For the same substrate, we obtained size (2% ALG-Na) > size (1% ALG-Na) > size (water). Compared to water, viscous liquid allowed more versatile control of droplet size, which can be tuned by both surface CAH and liquid viscosity.

The CAH-based strategy shows its uniqueness in design of surface for complicated hydrogel architectures compared to wettability-based way. To make comparison, we fabricated hydrophilic/hydrophobic and superhydrophilic/superhydrophobic substrates, hydrophobic/superhydrophobic (small-CAH/ultralow-CAH) and hydrophobic/superhydrophobic (large-CAH/ultralow-CAH) substrates (Table S2, Supporting Information). For hydrophilic/hydrophobic substrates, the hydrophobic background had a larger CAH than superhydrophobic background, leading to increased hysteresis force during dip-coating. When liquid (3 wt% ALG-Na) was more viscous than what we employed above, it stuck to the hydrophobic background. On the other hand, for superhydrophilic/superhydrophobic substrate, although ALG-Na solution was compartmentalized, the size of droplets could not be varied. Hydrophobic/superhydrophobic substrates, however, allowed compartmentalization of liquids with controlled size by different CAH. The ultralow-CAH background resisted sticking of liquids, while controlled-CAH patterns tuned the size of droplets.

2.3. Fabrication of Semi-Egg-Like Structures

In terms of controllable droplet size and rapid-gelation characteristics of ALG-Na by Ca^{2+}, we fabricated alginate hydrogel

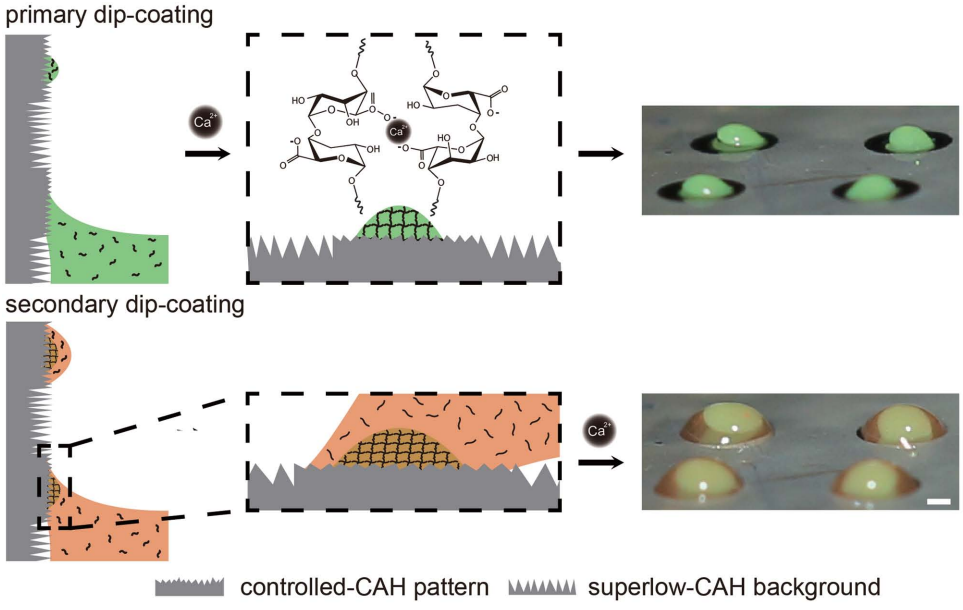

Figure 3. Fabrication of semi-egg-like hydrogel architecture. By dip-coating in ALG-Na solution (stained green), droplets with controlled size were formed on the patterns. Immersing substrates in $CaCl_2$ solutions (5 wt%) led to rapid gelation of droplets. Secondary dip-coating substrate in ALG-Na solution (stained red) led to formation of droplets covering the patterns. The increased size of secondary droplets resulted from increased adhesion on hydrophilic ALG-Ca. Scale bar: 250 μm.

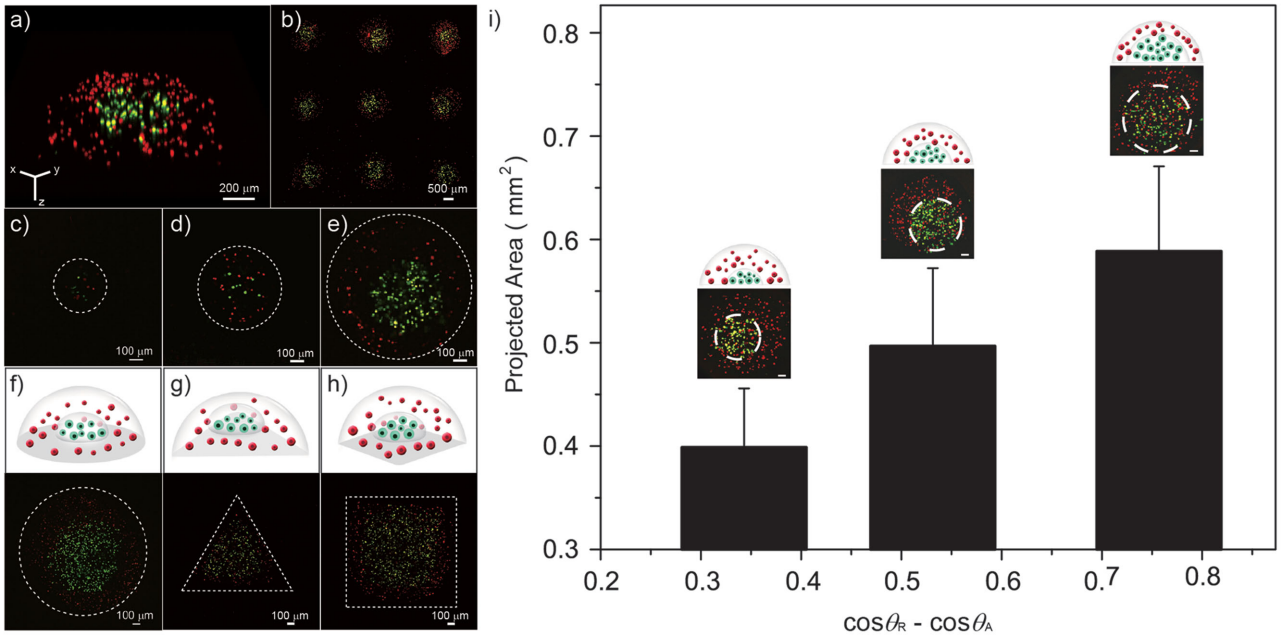

Figure 4. Heterogeneous compartmentalization of cells in semi-egg-like hydrogel. a) Confocal 3D reconstruction of a semi-egg-like hydrogel droplet with a tilt of 10°. MCF7 cells (green) were in the inner part, and NIH 3T3 cells (red) were in the outer part. b) Semi-egg-like cell encapsulated hydrogel droplets fabricated in arrays. c–f) Semi-egg-like structures with increasing the size of the outer part with diameter from 0.25, 0.5, 1, and 2 mm. g,h) Semi-egg-like structures with triangular and rectangular shape. i) Using controlled-CAH/ultralow-CAH substrates with $\cos\theta_R - \cos\theta_A$ 0.34 ± 0.03, 0.53 ± 0.04, and 0.75 ± 0.04, size of inner part of semi-egg-like architecture varied from 0.40 ± 0.06, 0.50 ± 0.08 to 0.59 ± 0.08 mm^2 (projected area). Scale bar: 100 μm.

droplets with a semi-egg-like architecture. As shown in **Figure 3**, by performing primary dip-coating, ALG-Na droplets were formed on controlled-CAH patterns. The addition of Ca^{2+} resulted in rapid gelation of ALG-Na into calcium alginate (ALG-Ca), due to electrostatic interaction between Ca^{2+} and alginate molecules.[17] After secondary dip-coating, another ALG-Na solution covered the as-patterned droplets. We believed that the increased size of secondary droplet was due to increased affinity from hydrophilicity of as-formed hydrogel, compared to bare patterns. During secondary dip-coating, the increased affinity from hydrogel droplet added to hysteresis force from pattern, resulting in an increased size of the outer layer. Final gelation led to formation of the semi-egg-like architecture.

2.4. Cell Encapsulated Semi-Egg-Like Structures for Cytotoxicity Test

To achieve controlled cell compartmentalization, we employed cell-encapsulated ALG-Na solution in fabricating semi-egg-like structure using the protocol as described above (**Figure 4**). Figure 4a shows a tilted view of 3D reconstructed confocal image, with MCF7 cells (green) surrounded by NIH 3T3 cells (red). Figure 4b shows the semi-egg-like hydrogel patterned in arrays. We further demonstrated that the semi-egg-like hydrogel allowed flexible control of size by different CAH and sizes of patterns. For the outer part, we fabricated four patterns with the same CAH (0.34 ± 0.03), but varied diameters from 0.25, 0.5, 1.0 to 2.0 mm by photolithography. We obtained semi-egg-like architectures with increasing size of whole droplet (Figure 4c–f). Also we fabricated triangular and rectangular shape of semi-egg-like droplets (Figure 4g,h). For controlling the inner part of the semi-egg-like hydrogel, we employed substrates with the same diameter (1.0 mm), but varied CAH (values of $\cos\theta_R - \cos\theta_A$ were 0.34 ± 0.03, 0.53 ± 0.04, and 0.76 ± 0.04). Sizes of inner part obtained varied from 0.40 ± 0.06, 0.50 ± 0.08 to 0.59 ± 0.08 mm^2 (projected area) (Figure 4i). The viability of cells (both inner part and outer part) after 5 d of culturing was 92% ± 3% (Figure S5, Supporting Information), which was determined by the live/

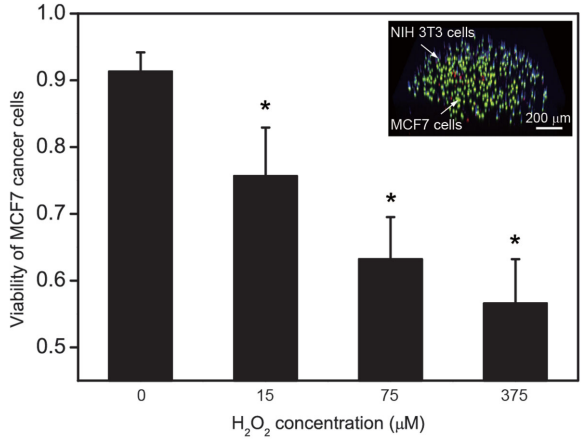

Figure 5. Viability of MCF7 cells in semi-egg-like hydrogel in response to H_2O_2. After H_2O_2 treatment for 2 h and stained by live/dead assay. To identify MCF7, NIH 3T3 cells were stained in blue before fabricating the structure. The asterisk * indicated that $p < 0.05$, which is statistically different between cells treated with H_2O_2 and control experiment. Inset: Confocal fluorescent images of cells with a tilt of 10°.

dead assay.[6] Cells were round in the hydrogel matrix, and the proliferation was suppressed by comparing the number of live cells at 5 d with that at 0 d.

The semi-egg-like structure could serve as a simplified model for studying cellular response to oxidative stress in vivo. As a proof of concept, we examined the viability of MCF7 cells surrounded by NIH 3T3 cells after treatment with H_2O_2. H_2O_2 is a reactive oxygen species (ROS) that can induce apoptosis, thus widely used as a positive control for nanodrugs. From **Figure 5** and Figure S6 (Supporting Information), viability of MCF7 cells was obviously affected by the addition of H_2O_2, and decreased in a dose-dependent manner. We believe that the semi-egg-like structure may hold promises for biomedical applications such as tissue engineering and drug screening.

3. Conclusion

In conclusion, a CAH-based strategy for size-controlled fabrication of cell-encapsulated semi-egg-like architecture was demonstrated. Compared to conventional substrates designed with wettability contrast, the controlled-CAH/ultralow-CAH substrate can compartmentalize water as well as cell-encapsulated viscous liquid with controlled size, which is crucial for engineering local structures in compartments. While the present approach is hard to control patterns of single cells and oligo cells with precise shape, spreading area, and cell–cell contact like some other approaches,[30–33] it is very efficient to pattern multiple cells based on CAH. Using the compartmentalized cells as a simplified model, we demonstrate that it can be used for biological applications such as cytotoxicity test. We believe that the CAH-based strategy would offer more opportunities to versatile design of cell-encapsulated complex structures for tissue engineering, as well as other applications such as inkjet printing,[19] digital microfluidics,[34] and water collection.[35]

4. Experimental Section

Reagents and characterization details are provided in the Supporting Information.

Etching Silicon with Various Roughness: Surface roughness of silicon was adjusted by various etching conditions. Before etching, silicon substrates (1 cm × 1 cm, cut from wafers) were rinsed in ethanol and acetone for 10 min, respectively, and treated by boiling H_2SO_4 and H_2O_2 solution (3:1, v/v, *Caution! The Piranha solution is harmful for skin, and should be handled carefully!*) for 30 min. Afterward, the substrates were rinsed in deionized water (Milli-Q water, 18.2 MΩ) for three times. Following previous methods,[26,27] $AgNO_3$ and HF solutions were used as etching solution. A series of $AgNO_3$ and HF solutions with different concentrations were prepared by diluting the original solution (0.17 g $AgNO_3$ in 10 mL HF and 55 mL deionized water) in deionized water. The dilution ratios were 1:4, 2:3, 3:2, and 4:1, respectively. Also the original solution was used. Silicon substrates were immersed in various etching solutions for 20 s, followed by removing silver film in HNO_3 solutions (30%, v/v) for 5 min. After rinsing in deionized water for three times, the substrates were dried in oven (80 °C) for 1 h.

Fabrication of Controlled-CAH/Ultralow-CAH Substrates: Silicon wafers were first etched at different concentrations of etching solutions and dried. As shown in Figure S2 (Supporting Information), photolithography was performed to pattern wafers. After development, patterned areas were covered with photoresist. The wafers were further cut into 1 cm × 1 cm substrates. The substrates were immersed in $AgNO_3$ and HF etching solution for 10 min. The exposed regions were etched while photoresist-protected area was not etched. After etching, substrates were rinsed in deionized water. Acetone was used to remove photoresist. Substrates were then dried by a nitrogen gun and further in oven (80 °C) for 1 h. Finally, all substrates were modified with OTS (dissolved in toluene in 0.2%, v/v, 10 min).

Fabrication of Semi-Egg-Like Cell-Encapsulated Hydrogel: MCF7 cancer cells and NIH 3T3 fibroblast were employed as model cells. Before dispersed in alginate solution, MCF7 cells were labeled with calcein AM (green) and NIH 3T3 cells were labeled with CellTracker Orange CMRA (red), according to manufacturer's protocol. After suspending and centrifugation, both cells were dispersed in alginate solution (2 wt% in PBS) with a density of 1×10^6 cells mL^{-1}. The substrates were dipped in MCF7 cell encapsulated solution for 30 s, and dragged out at a speed of 1 mm s^{-1}. The substrates were then immersed in $CaCl_2$ solution (5 wt%) for 5 s for gelation. After that, they were rinsed in PBS for three times. The substrates were again immersed in fibroblast cell encapsulated solution for 30 s, dragged out at a speed of 1 mm s^{-1}, and gelled under the same conditions as above.

Cytotoxicity Test by H_2O_2: NIH 3T3 cells were stained in blue by Hoechst. After 30 min, both NIH 3T3 cells and MCF7 cells were encapsulated into the semi-egg-like structure, with MCF7 in the inner part and NIH 3T3 cells in the outer part. Substrates were treated with cell-encapsulated semi-egg-like structures with H_2O_2 (15, 75, and 375×10^{-6} M) for 2 h. After that, we rinsed the substrates in PBS for three times, and performed the live/dead assay. Confocal fluorescent microscopy was used to capture cells. Finally, the MCF7 cells (without blue emissions) were counted and the viability was calculated.

Supporting Information

Supporting Information is available from the Wiley Online Library or from the author.

Acknowledgements

This research was supported by the National Research Fund for Fundamental Key Projects (2012CB933800 and 2013CB933000), National Natural Science Foundation (21175140, 21425314, 21434009, and 21421061), the Key Research Program of the Chinese Academy of Sciences (KJZD-EW-M01), the National High Technology Research and Development Program of China (863 Program) (2013AA032203), MOST (2013YQ190467), and China Postdoctoral Science Foundation Funded Project (2012M510555 and 2013T60176). The authors are grateful for the discussion and help from Dr. M. Gao, Dr. J. L. Tang, and Prof. Y. Liu.

Received: April 15, 2015
Revised: May 19, 2015
Published online: June 12, 2015

[1] M. Meier, R. V. Sit, S. R. Quake, *Proc. Natl. Acad. Sci. U.S.A.* **2013**, *110*, 477.
[2] L. Dong, A. K. Agarwal, D. J. Beebe, H. R. Jiang, *Nature* **2006**, *442*, 551.
[3] a) F. Deiss, W. L. Matochko, N. Govindasamy, E. Y. Lin, R. Derda, *Angew. Chem. Int. Ed.* **2014**, *53*, 6374; b) F. Deiss, W. L. Matochko, N. Govindasamy, E. Y. Lin, R. Derda, *Angew. Chem.* **2014**, *126*, 6492.
[4] H. Tekin, J. G. Sanchez, C. Landeros, K. Dubbin, R. Langer, A. Khademhosseini, *Adv. Mater.* **2012**, *24*, 5543.

[5] M. B. Oliveira, G. M. Luz, J. F. Mano, *J. Mater. Chem. B* **2014**, *2*, 5627.
[6] M. B. Oliveira, A. I. Neto, C. R. Correia, M. I. Rial-Hermida, C. Alvarez-Lorenzo, J. F. Mano, *ACS Appl. Mater. Interfaces* **2014**, *6*, 9488.
[7] E. Ueda, F. L. Geyer, V. Nedashkivska, P. A. Levkin, *Lab Chip* **2012**, *12*, 5218.
[8] A. N. Efremov, E. Stanganello, A. Welle, S. Scholpp, P. A. Levkin, *Biomaterials* **2013**, *34*, 1757.
[9] B. Su, S. T. Wang, J. Ma, Y. L. Song, L. Jiang, *Adv. Funct. Mater.* **2011**, *21*, 3297.
[10] J. Seo, J. S. Lee, K. Lee, D. Kim, K. Yang, S. Shin, C. Mahata, H. B. Jung, W. Lee, S. W. Cho, T. Lee, *Adv. Mater.* **2014**, *26*, 7043.
[11] D. Quéré, *Annu. Rev. Mater. Res.* **2008**, *38*, 71.
[12] L. C. Gao, T. J. McCarthy, *Langmuir* **2006**, *22*, 6234.
[13] D. Bonn, J. Eggers, J. Indekeu, J. Meunier, E. Rolley, *Rev. Mod. Phys.* **2009**, *81*, 739.
[14] J. V. I. Timonen, M. Latikka, O. Ikkala, R. H. A. Ras, *Nat. Commun.* **2013**, *4*, 2398.
[15] M. J. Liu, Y. M. Zheng, J. Zhai, L. Jiang, *Acc. Chem. Res.* **2010**, *43*, 368.
[16] T. L. Sun, L. Feng, X. F. Gao, L. Jiang, *Acc. Chem. Res.* **2005**, *38*, 644.
[17] X. J. Liu, Y. M. Liang, F. Zhou, W. M. Liu, *Soft Matter* **2012**, *8*, 2070.
[18] K. G. Winkels, I. R. Peters, F. Evangelista, M. Riepen, A. Daerr, L. Limat, J. H. Snoeijer, *Eur. Phys. J.: Spec. Top.* **2011**, *192*, 195.
[19] M. X. Kuang, L. B. Wang, Y. L. Song, *Adv. Mater.* **2014**, *26*, 6950.
[20] J. Z. Chen, S. M. Troian, A. A. Darhuber, S. Wagner, *J. Appl. Phys.* **2005**, *97*, 014906.
[21] D. Noguera-Marin, C. L. Moraila-Martinez, M. A. Cabrerizo-Vilchez, M. A. Rodriguez-Valverde, *Langmuir* **2014**, *30*, 7609.
[22] D. Huh, G. A. Hamilton, D. E. Ingber, *Trends Cell Biol.* **2011**, *21*, 745.
[23] A. Dolatshahi-Pirouz, M. Nikkhah, A. K. Gaharwar, B. Hashmi, E. Guermani, H. Aliabadi, G. Camci-Unal, T. Ferrante, M. Foss, D. E. Ingber, A. Khademhosseini, *Sci. Rep.* **2014**, *4*, 3896.
[24] M. P. Lutolf, R. Doyonnas, K. Havenstrite, K. Koleckar, H. M. Blau, *Integr. Biol.* **2009**, *1*, 59.
[25] D. R. Albrecht, G. H. Underhill, T. B. Wassermann, R. L. Sah, S. N. Bhatia, *Nat. Methods* **2006**, *3*, 369.
[26] K. Q. Peng, Y. J. Yan, S. P. Gao, J. Zhu, *Adv. Mater.* **2002**, *14*, 1164.
[27] M. L. Zhang, K. Q. Peng, X. Fan, J. S. Jie, R. Q. Zhang, S. T. Lee, N. B. Wong, *J. Phys. Chem. C* **2008**, *112*, 4444.
[28] R. Fijan, M. Basile, S. Sostar-Turk, E. Zagar, M. Zigon, R. Lapasin, *Carbohydr. Polym.* **2009**, *76*, 8.
[29] J. A. Rowley, G. Madlambayan, D. J. Mooney, *Biomaterials* **1999**, *20*, 45.
[30] X. Yao, R. Peng, J. D. Ding, *Adv. Mater.* **2013**, *25*, 5257.
[31] B. Cao, R. Peng, Z. H. Li, J. D. Ding, *Biomaterials* **2014**, *35*, 6871.
[32] R. Peng, X. Yao, J. D. Ding, *Biomaterials* **2011**, *32*, 8048.
[33] X. Wang, S. Y. Li, C. Yan, P. Liu, J. D. Ding, *Nano Lett.* **2015**, *15*, 1457.
[34] M. J. Jebrail, M. S. Bartsch, K. D. Patel, *Lab Chip* **2012**, *12*, 2452.
[35] Y. M. Zheng, H. Bai, Z. B. Huang, X. L. Tian, F. Q. Nie, Y. Zhao, J. Zhai, L. Jiang, *Nature* **2010**, *463*, 640.